RESEARCH PAPERS

Acta Cryst. (1996). A**52**, 125–132

Approximants and Intermediate Stages during Transformation from a Quasicrystalline to a Crystalline Phase in an Al–Mn–Si Alloy

V. HANSEN* AND J. GJØNNES

Department of Physics, University of Oslo, PO Box 1048 Blindern, 0316 Oslo, Norway

(*Received 5 May 1995; accepted 23 August 1995*)

Abstract

In precipitate particles formed by heat treatment of industrially cast Al–(1.8–1.6wt%)Mn alloys, a sequence of stages intermediate between the quasicrystalline I phase and the cubic α-AlMnSi phase have been found. Their electron diffraction patterns and images can be interpreted in terms of faults on $\{110\}_\alpha$ planes, with a fault vector $[\bar{3}50]/16$ or $[\bar{1}\tau 0]/2\tau^2$, where $\tau = 1.618$ is the golden mean. A lattice generated by such faults on every $(110)_\alpha$ plane has as its unit cell a prolate rhombohedron (α') that is complementary to the oblate rhombohedron (α) that describes the packing of the MacKay icosahedra in α-AlMnSi. Domains of this new lattice have been observed. Based on the two rhombohedra, a cubic $Pa3$ structure model (α'') with cell dimension τ times α-AlMnSi and nearest-neighbour intericosahedral vectors along all threefold axes of the icosahedron is proposed as a second approximant to the I phase in the system, with α-AlMnSi as the first approximant. Calculations of diffraction patterns and Patterson sections are presented as support for this proposal.

1. Introduction

Relations between quasicrystalline and crystalline phases with similar compositions were discussed shortly after the original discovery of the icosahedral phase in the Al–Mn and Al–Mn–Si systems by Shechtman, Blech, Gratias & Cahn (1984), see also Elser & Henley (1985) and Guyot & Audier (1985). Transformations from the AlMnSi I phase to the cubic α-AlMnSi (Cooper & Robinson, 1966) or the orthorhombic Al_6Mn (Nicol, 1953) phase were studied by Pannetier, Dubois, Janot & Bilde (1987), Koskenmaki, Chen & Rao (1986) and others. Similarities in the intensity distribution in their diffraction patterns were taken as an indication that the I and α phases contain the same basic building block, *viz* the Mackay icosahedron; an object consisting of 54 atoms: 12Mn + 42(Al + Si) (Guyot & Audier, 1985; Cahn, Gratias & Mozer, 1988*a*,*b*; Duneau & Oguey, 1989; Robertson & Moss, 1991; Yamamoto & Hiraga, 1988). The α phase is termed an approximant to the Al–Mn–Si quasicrystal (Mukhopadyay, Ishihara & Ranganathan 1991), and is used as a guide to the atomic decoration on the quasilattice. The intermediate stages appearing during the $I \rightarrow \alpha$ transformation are thus of particular interest; they may reveal ways of packing the Mackay icosahedra, other than the b.c.c.-like arrangement characteristic of the α phase.

Table 1. *Orientation relations between axes in the icosahedron and approximate directions in the α phase and aluminium matrix*

F.c.c. matrix	Icosahedron	α-AlMnSi
[110], [311]	Fivefold axis	[530]
[111], [31$\bar{2}$]	Threefold axis	[111], [5$\bar{3}$0]
[511], [4$\bar{3}$2]		
[1$\bar{1}$0], [11$\bar{1}$]	Twofold axis	[100], [312]
[211], [51$\bar{1}$]		

In an electron-microscopy study of precipitate particles, so-called dispersoids, formed by heat treatment of industrially cast aluminium alloys with relatively high Mn content, we found many particles belonging to this intermediate stage. The dispersoid system was seen to develop through the sequence

$$\text{solid solution} \rightarrow I \text{ phase} \rightarrow \alpha \text{ phase} \rightarrow Al_{12}Mn$$

with characteristic orientation relationships between the different structures (Hansen, Gjønnes & Andersson, 1989) (Table 1). The stable phase $Al_{12}Mn$ (Adam & Rich, 1954), which appears after prolonged annealing, has a body-centred cubic arrangement of 13-atom icosahedra with Mn in the centre. Electron-microscope observations indicated that $Al_{12}Mn$ was nucleated on α-phase particles, with a definite orientation relationship.

Energy-dispersive spectroscopy (EDS) analysis indicated only small changes in composition during the transition from I to α. It was found that diffraction patterns and images from these can be interpreted by a set of structures built from two complementary rhombohedral units. One of them is the primitive unit cell of the (nearly) b.c.c. α-AlMnSi phase, *i.e.* an oblate rhombohedron with trigonal axis $[111]/2$ and edges along the three $[11\bar{1}]/2$ *etc.* referred to the cubic unit cell of α and rhombohedral angle 109.47° [= $\arccos(-1/3)$].

The other, prolate, rhombohedron has the same edge length, *viz* 10.88 Å, and the rhombohedral angle $\alpha = 70.53°$ [$= \arccos(1/3)$]; it was found as the trigonal unit cell in small domains within partly transformed dispersoid particles in the heat-treated alloy. The two rhombohedra have the same rhombic faces; the rhombohedral angles 70.53 and 109.47° correspond to angles between threefold axes in the icosahedron as well as in the cube. As is well known, the twelve threefold axes of the icosahedron correspond to the four body diagonals $\langle 111 \rangle$ and eight $\langle \tau^2 10 \rangle$ directions in the cube, τ is the golden mean ($= 1.618$). The above rhombohedra are seen to be different from the three-dimensional Penrose tiles (Amman rhombohedra), which are commonly used as building tiles in the description of icosahedral quasicrystals (Henley & Elser, 1986). The relation between the Amman rhombohedra, which have edges pointing along fivefold directions of an icosahedron and the rhombohedra similar to the present ones has been discussed by Dmitrienko (1994). Cheng & Gjønnes (1994) have shown how the above rhombohedral unit cells can be derived as approximants to the icosahedral quasilattice by a strip-projection approach.

In the two rhombohedral elements, the edges of length 10.88 Å along triads and the short face diagonal 12.68 Å correspond to the nearest and next-nearest distance between MacKay icosahedra in the crystalline as well as in the quasicrystalline structure. In the following, we present diffraction patterns and micrographs that can be interpreted in terms of these elements and discuss their use in the description of quasicrystalline structure. The development of the particle system during annealing treatment of the alloy is described elsewhere (Hansen, Andersson, Tibballs & Gjønnes, 1995); here we concentrate on the crystallographic relations between the structures that appear.

2. Experimental

The material was an experimental alloy of composition 97.9% Al, 1.59% Mn, 0.29% Fe, 0.09% Si, which had been strip-cast by Hydro Aluminium, Årdal. After deformation by cold rolling, the strip was heat treated in a salt bath at different temperatures in the interval 573–773 K; the annealing time was varied from a few seconds up to 1000 h. Thin foils prepared by electrolytic thinning in a standard way were examined in JEM 200CX and JEM 2000FX electron microscopes equipped with energy-dispersive spectrometers. Composition analyses were carried out on particles extracted in butanol by the

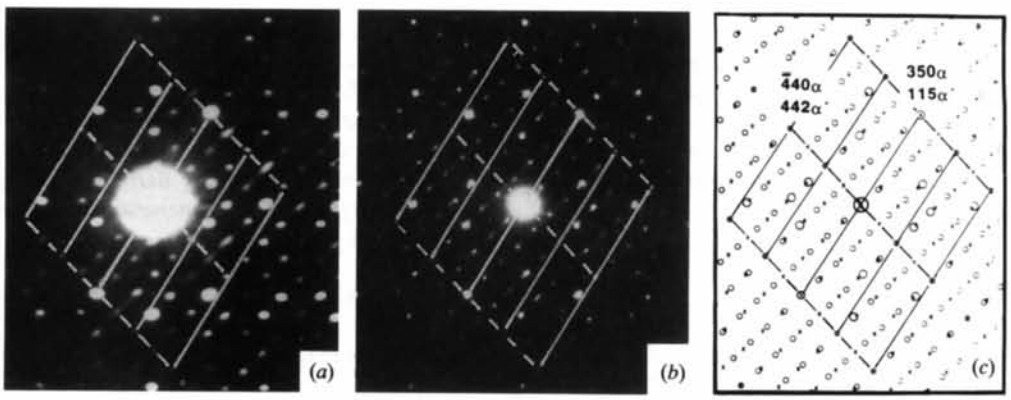

Fig. 1. (*a*) Diffraction pattern with diffuse $\langle 110 \rangle_\alpha$ streaks, from a particle in the intermediate stage between *I* and α phases, $[001]_\alpha$ projection. (*b*) Diffraction pattern, $[001]_\alpha$ projection, with two sets of spots, indexed by α and α' lattices, as shown in (*c*).

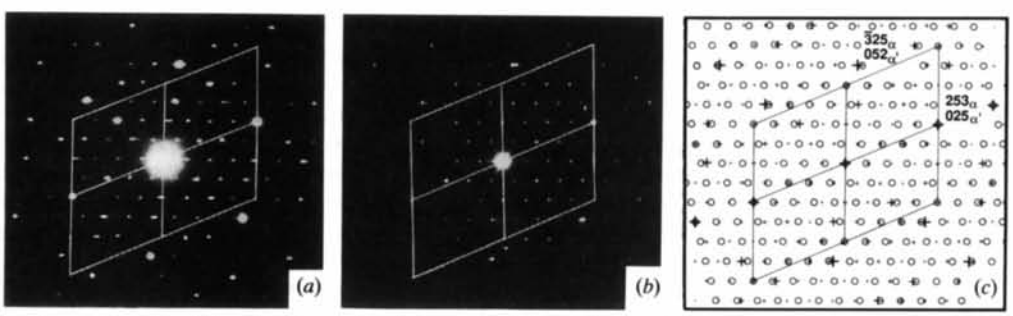

Fig. 2. (*a*) Diffraction pattern with diffuse $\langle 110 \rangle_\alpha$ streaks, from a particle in the intermediate stage between *I* and α phases, $[1\bar{1}1]_\alpha$ projection. (*b*) Diffraction pattern, $[1\bar{1}1]_\alpha$ projection with two sets of spots, indexed by α and α' lattices, as shown in (*c*).

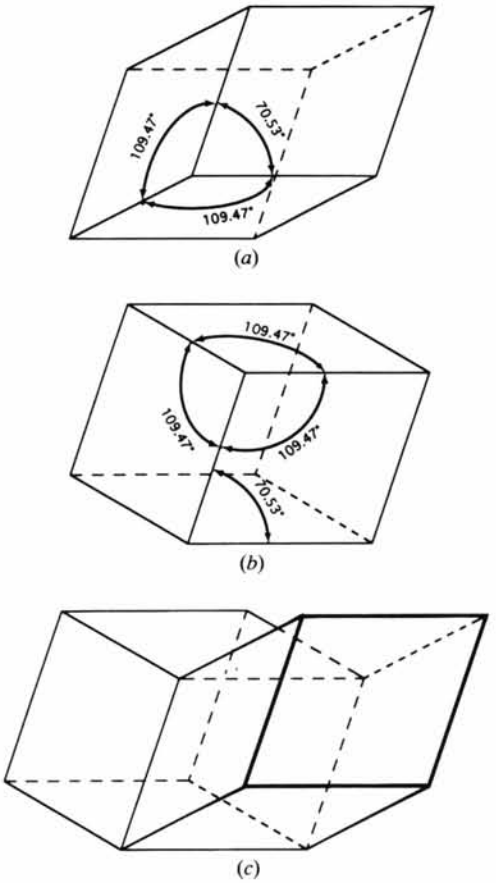

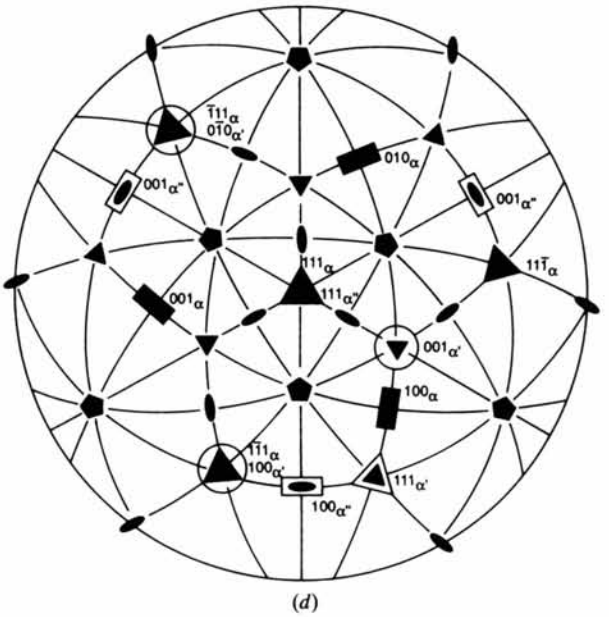

Fig. 3. (*a*) Oblate rhombohedron formed from centres of MacKay icosahedra in the α phase. (*b*) Prolate rhombohedron formed from centres of MacKay icosahedra in the α' phase. (*c*) Face sharing between a prolate and an oblate rhombohedron. (*d*) Stereographic projection showing orientation of the two lattices relative to the icosahedral axes.

method described by Simensen, Fartum & Andersen (1984).

3. Results

Dispersoid particles, typically of diameter 20–50 nm, found in the thin-foil specimens after a few seconds heat treatment gave electron diffraction patterns characteristic of the quasicrystalline *I* phase. For the smallest particles, slight deviations from icosahedral symmetry were common. Upon further heat treatment, the particles increased in size and transformed to crystalline phases according to the sequence: solid solution $\rightarrow$ *I* phase $\rightarrow$ α phase $\rightarrow$ $Al_{12}Mn$.

The $I \rightarrow \alpha$ transformation proceeds through an intermediate stage that contains extensive faults as revealed by diffuse $\langle 110 \rangle_\alpha$ streaks in the electron diffraction selected-area diffraction (SAD) patterns, see Figs. 1(*a*) and 2(*a*), which are taken along $[001]_\alpha$ and $[1\bar{1}1]_\alpha$ directions, respectively. From patterns taken in several projections, the fault vector on (110) planes was determined to be $\delta = [\bar{3}50]/16$, which is along a fivefold direction in the MacKay icosahedron and has a component normal to the fault plane (110). The same

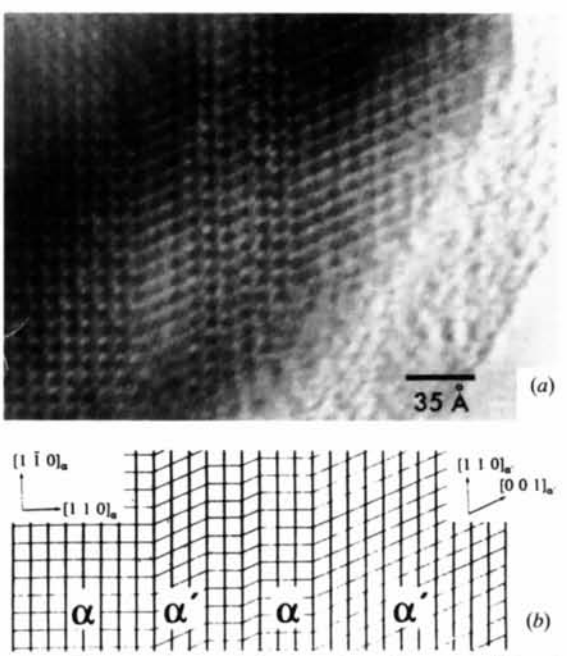

Fig. 4. (*a*) Electron micrograph from particle with α and α' domains, as sketched in (*b*).

fault vector was identified by Andersen, Guo & Høier (1990) from high-resolution electron-microscopy images of single faults in the α phase. The Brillouin zone for the diffuse scattering corresponding to δ is indicated in Fig. 1(*a*). Some of the α spots are seen to be displaced along the $\langle 110\rangle_\alpha$ direction, as is indeed expected for a fault-vector component normal to the fault plane, see the discussion by Cowley (1976). Other patterns (Figs. 1*b*, 2*b*) contain two distinct sets of diffraction spots. One of the two corresponds to the α phase, the other set (α') is indexed according to a rhombohedral lattice that can be produced from the α phase by a fault δ on every (110) plane (see Fig. 1*c*). The resulting two lattices and the relation between them are shown in Fig. 3 together with a stereographic projection of the orientations relative to the cube and the icosahedron.

Table 2. *Orientation relations between the two rhombohedra (α, α') and the icosahedron*

$$[001]_{\alpha'} \parallel [\tau^2 10]_\alpha$$
$$[100]_{\alpha'} \parallel [1\bar{1}1]_\alpha$$
$$[010]_{\alpha'} \parallel [1\bar{1}\bar{1}]_\alpha$$
$$[111]_{\alpha'} \parallel [\tau^2 \bar{1}0]_\alpha$$
$$[110]_{\alpha'} \parallel [001]_\alpha$$

The micrograph Fig. 4(*a*) of a dispersoid particle is consistent with such a lattice, *cf.* the sketch in Fig. 4(*b*). An intergrowth of the two structures is seen: α', with a unit cell described as a prolate rhombohedron, and the (nearly) b.c.c. α-AlMnSi, with the primitive unit cell described by an oblate rhombohedron complementary to the former. The orientation relations derived from

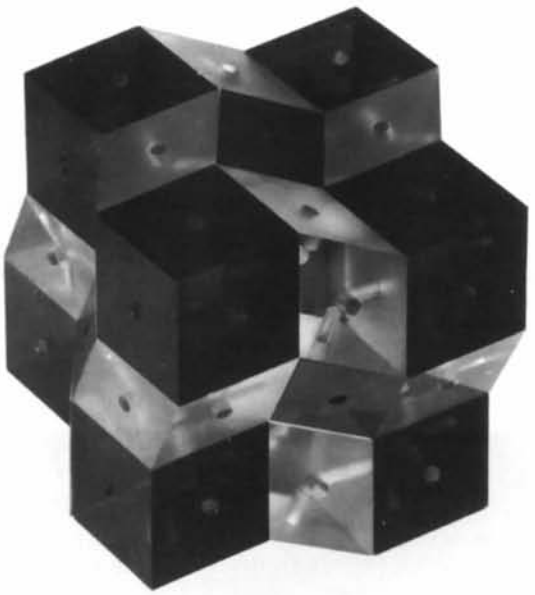

(*a*)

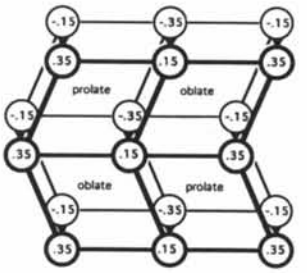

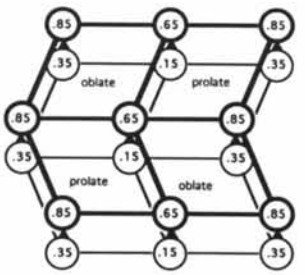

(*b*)

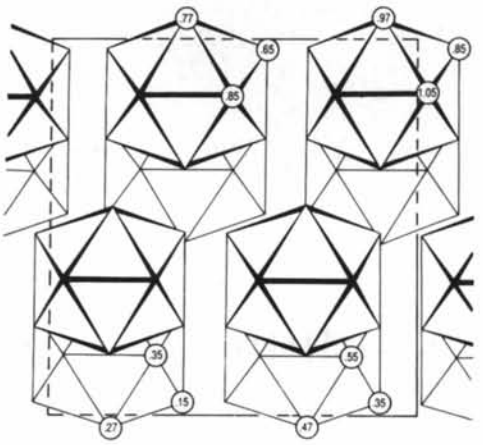

(*c*)

Fig. 5. (*a*) Photograph of a model composed of oblate (dark) and prolate (light) rhombohedra. With MacKay icosahedra at the corners and including glue atoms, this unit will contain *ca* 500 atoms. (*b*) Two layers of the structure model seen along a cube axis with MacKay icosahedra at the corners. (*c*) Packing of MacKay icosahedra in the cubic α'' structure.

the diffraction patterns, Figs. 1 and 2, are summarized in Table 2: the edges of the two rhombohedra as well as their trigonal axes are parallel to triads in the MacKay icosahedron of α-AlMnSi. If we assume MacKay icosahedra at the corners also in the α' unit, the nearest-neighbour distance between the icosahedra along their threefold directions will be the same. The two rhombohedra fit together in the $(110)_\alpha$ fault plane. The acute angle 70.53° between edges forming the rhombic faces appears as the rhombohedral angle of α', whereas the obtuse supplement angle 109.47° is the rhombohedral angle of α', *cf.* Fig. 3. Note that the α' lattice of MacKay icosahedra is similar to the $A10$-type rhombohedral lattice of Hg.

4. Discussion

The diffraction patterns and micrographs presented here from the transition stage in the $I \rightarrow \alpha$ transformation of the dispersoids can be interpreted by the two rhombohedral elements described above, *viz* the primitive rhombohedral cell, which corresponds to the α-AlMnSi structure, and a new rhombohedral unit, α', which is complementary to α. The similarity between diffraction patterns from α-AlMnSi and the I phase has been noted by several researchers; a similar relation is apparent between the α'- and I-phase patterns. The I phase may in fact appear as intermediate between the two, as is illustrated further by the comparison of their diffraction patterns along twofold axes (Fig. 1): the strong spots have similar positions to those of the twofold projection of the I phase.

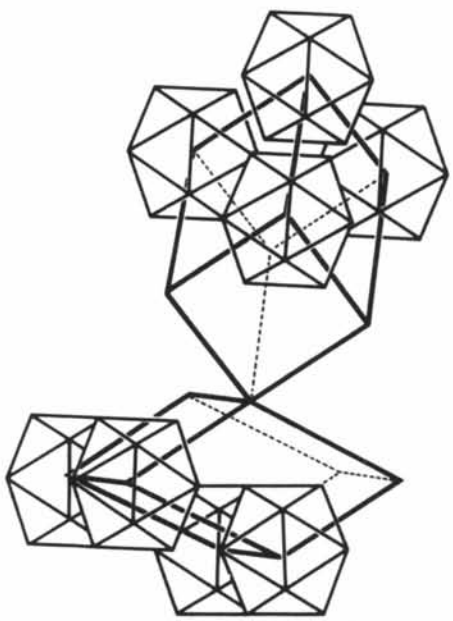

Fig. 6. Schematic representation of the α and α' rhombohedra with a common trigonal axis.

These observations raise the question: Can a quasicrystalline structure be constructed from the above pair of prolate and oblate rhombohedra? From general crystallographic considerations, Dmitrienko (1993, 1994) has recently proposed a description of quasicrystals in terms of similar (but smaller) rhombohedra. The prolate and oblate rhombohedra can be joined in different ways so as to illustrate different packings of MacKay icosahedra. The model in Fig. 5 shows an example of a periodic structure (α''), constructed as a space-filling packing of alternating oblate and prolate rhombohedra. In the model, there are four rhombohedra of each kind, and hence four MacKay icosahedra, in a cubic unit cell (Figs. 5*b*, *c*). Rhombohedra of opposite kind share faces and meet at corners with a common trigonal axis, see Fig 6; rhombohedra of the same type share edges. The cubic unit cell of the model has a lattice constant τ ($= 1.618$) times the unit cell of α-AlMnSi and the space group $Pa3$ with MacKay icosahedra at the corners. The mathematical relation between the axes of the new unit cell and α-AlMnSi can be represented by the matrix

$$\begin{bmatrix} \tau & \tau^2 & \bar{1} \\ \tau^2 & \bar{1} & \tau \\ \bar{1} & \tau & \tau^2 \end{bmatrix} \Big/ 2\tau^2 \approx \begin{bmatrix} 8 & 13 & \bar{5} \\ 13 & \bar{5} & 8 \\ \bar{5} & 8 & 13 \end{bmatrix} \Big/ 16. \quad (1)$$

With MacKay icosahedra placed at the eightfold positions $8(c)$, 0.154, 0.154, 0.154, where four rhombohedra share corners, and with the same orientations as in the α structure, each icosahedron will be connected to neighbours along seven of their threefold axes. All triads in the icosahedron (six $\langle \tau\ 1/\tau\ 0 \rangle$ and four $\langle 111 \rangle$ referred to the cube axes) will then occur as intericosahedral vectors, although not with equal frequency. This results in a much stronger icosahedral character than in cubic α-AlMnSi. The unit cell, with lattice constant close to 20 Å, will contain approximately 500 atoms when some 'glue' atoms are added, as in α-AlMnSi. If the α phase is termed a first approximant to the I phase, the model de-

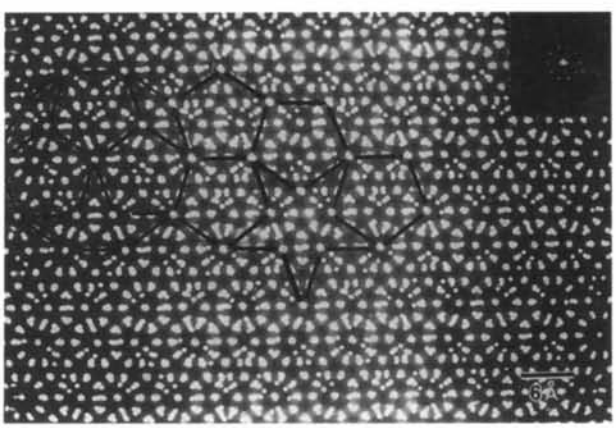

Fig. 7. A structure model corresponding to Fig. 5 (with point atoms) photographed along a quasi fivefold direction. The laser diffractogram is shown in the insert.

scribed above may be called a second approximant. The near-icosahedral symmetry of the structure is revealed by calculated projections, which resemble high-resolution images published in the literature, see *e.g.* Hiraga (1991); and also by optical diffractograms obtained from such projections; an example is shown in Fig 7.

The derivation of the three lattices α, α' and α'' as approximants to the *I* phase by a strip and projection method from a six-dimensional lattice is described by Cheng & Gjønnes (1994). The α'' lattice (Figs. 5 and 6) represents a packing of MacKay icosahedra with nearest-neigbour intericosahedral distances 10.88 Å along threefold axes of the icosahedron, next-nearest-neighbour distances 12.68 Å along twofold axes and distances 19.49 Å along fivefold axes of the icosahedron. The same intericosahedral distances are deduced from six-dimensional analysis (Cahn, Gratias & Mozer, 1988*b*), see also Duneau & Oguey (1989).

The symmetry of this packing is not fully icosahedral. However, higher-order approximants to an icosahedral structure can be constructed by repeating the procedure described by (1) or by the strip-projection procedure. It was found by Cheng & Gjønnes (1994) that this will create three further rhombohedra, and hence a local arrangement, which will entail incomplete or missing rhombohedra.

We have tested the main features of the proposed second-order approximant against the intensity data published by Gratias, Cahn & Mozer (1988) for *I*-AlMnSi by calculation of Patterson sections (*i.e.* two-dimensional sections of the normal three-dimensional vector space). The aim was to compare the packings of icosahedra; with this in mind, we divided the intensity data by the intensity function $I_I(\mathbf{q})$ calculated for an isolated MacKay icosahedron. It was expected that the main contribution to a Patterson function calculated in this

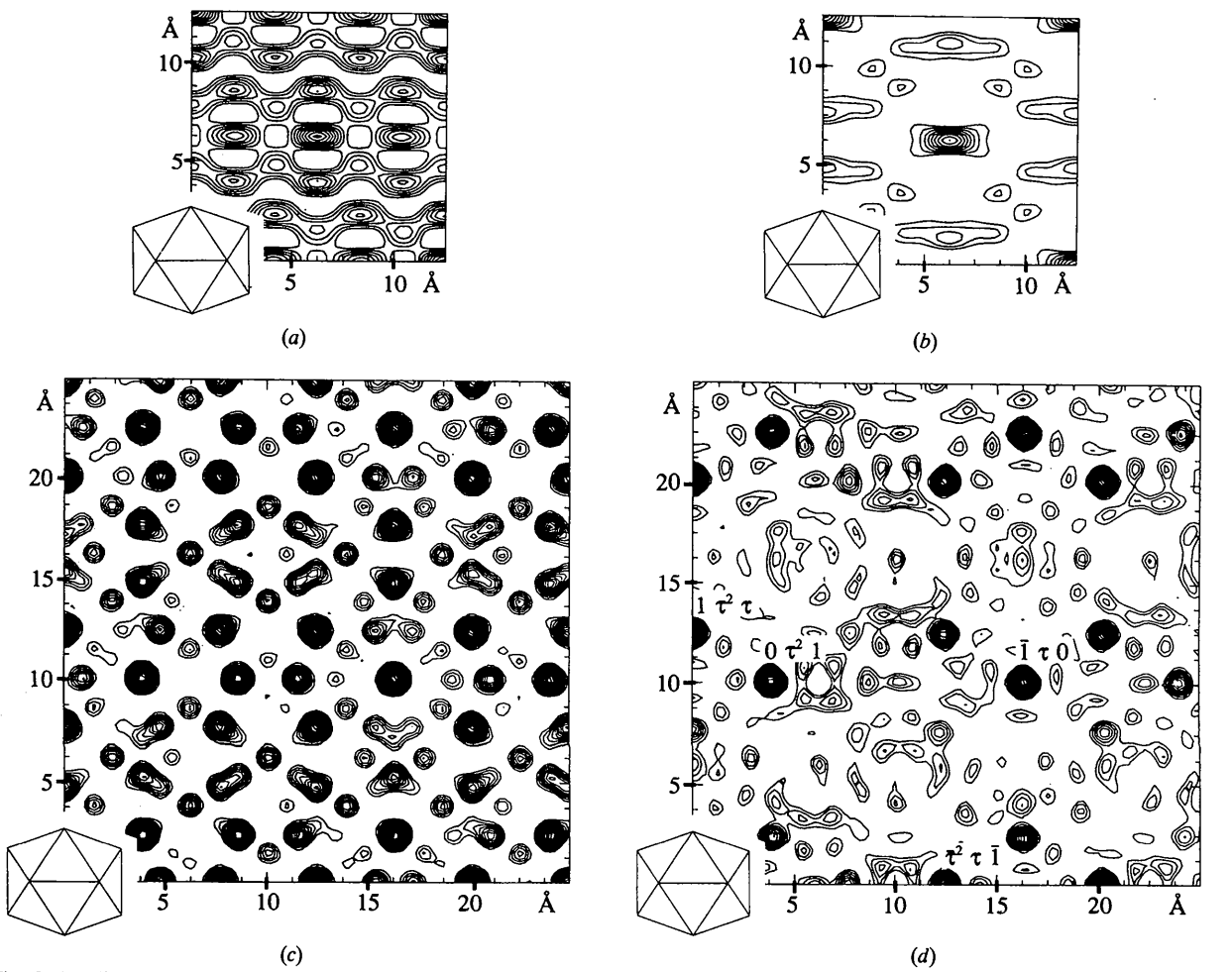

Fig. 8. (*a*), (*b*) Calculated [001] Patterson projection for cubic α-AlMnSi; (*c*), (*d*) Patterson section, normal to a twofold axis, for an AlMnSi quasicrystal, calculated from the data published by Gratias, Cahn & Mozer (1988). (*a*) and (*c*) calculated from the observed intensities, (*b*) and (*d*) calculated with intensities divided by the intensity function for a single MacKay icosahedron.

way will be from intericosahedral vectors. We checked this by first applying the procedure to the α-AlMnSi phase. Patterson projections $P(X, Y)$ calculated in the normal way and after the division by $I_I(\mathbf{q})$ are shown in Figs. 8(*a*) and (*b*). For Patterson calculations relating to the icosahedral phase, we translated the published intensities listed by the six indices hh', kk', ll' into indices HKL referred to a cubic system according to

$$H_j, K_j, L_j = (h + h'\tau, k + k'\tau, l + l'\tau)/A[2(2 + \tau)]^{1/2},$$

where A is the 6D icosahedral lattice parameter (Cahn, Gratias & Mozer, 1988*a*). By taking the relation between icosahedral and cubic symmetry into account, we could then calculate the Patterson section normal to a twofold axis of the icosahedron as

$$P(X, Y, 0) = \sum_j [I_j/I_I(\mathbf{q}_j)] \exp[2\pi i(H_j X + K_j Y)].$$

The calculations were performed in a cubic coordinate system, assuming $m3$ symmetry in Patterson space. We could then use the formulae for the cubic space group $Pm3$ by adding the extra icosahedral symmetry.

From the 58 published intensities, we then obtained the maps in Figs. 8(*c*), (*d*). Inspection of these maps revealed that the strong peaks correspond closely to the intericosahedral vectors of the 500-atom model proposed above. This result may be seen as confirming the assumption that the quasicrystalline AlMnSi contains MacKay icosahedra with a local environment, which can be described in terms of the two rhombohedra associated with the α and α' units.

However, for a further comparison of intensities, a model based on MacKay icosahedra alone is not sufficient. 132 'glue' atoms must be included in the unit cell in order to obtain a realistic atomic density. The position of the atoms within the α rhombohedra can reasonably be taken over from the α-AlMnSi structure. For 'glue' atoms within the α' rhombohedron, the positions must be chosen by some criterion. The packing of the icosahedra, as described by the two kinds of rhombohedron, is consistent with the space group $Pa3$. However, the icosahedra in the α phase are not perfect and identical (but retain the $m3$ symmetry). The non-centrosymmetric space group $P2_13$ was chosen rather than $Pa3$ in order to transfer the published α coordinates directly to the model.

The atomic positions for the models were deduced in this way: the axes were obtained by the transformation (1). In order to conform with the conventions of the space group $P2_13$, the origin should be at the mid-point between two icosahedra and was chosen at the centre of an oblate rhombohedron, which corresponds to the position $1/4, 1/4, 1/4$ in the unit cell of α. When α coordinates are transformed to the model by (1), a translation $-1/4\tau, -1/4\tau, -1/4\tau$ along the threefold axis must therefore be added. Next, we applied the symmetry operations of $P2_13$ to the new coordinates, noting that only one of the threefold axes in α-AlMnSi is retained through the transformation to the α'' structure. The next step was to fill the relatively large void in the centre of the prolate α' rhombohedron. This was acomplished by an icosahedral arrangement of aluminium atoms around the centre of the rhombohedron. The atomic positions were then adjusted until the closest interatomic distances were in the same range as in α-AlMnSi (Table 3). This led to 8 manganese and 39 aluminium positions in the asymmetric unit, which generated 564 atoms in the unit cell. The atomic density of this cell is 0.3% higher than in the α-AlMnSi phase.

Table 3. *Fractional coordinates for the α'' structure*

Atom	x	y	z
Mn(1)	0.05	0.97	0.85
Mn(2)	0.85	0.05	0.72
Mn(3)	0.84	0.64	0.97
Mn(4)	0.64	0.72	0.85
Mn(5)	0.96	0.03	0.16
Mn(6)	0.15	0.96	0.27
Mn(7)	0.16	0.35	0.03
Mn(8)	0.35	0.28	0.15
Al(1)	0.96	0.03	0.78
Al(2)	0.73	0.66	0.92
Al(3)	0.04	0.97	0.23
Al(4)	0.27	0.34	0.08
Al(5)	0.95	0.91	0.85
Al(6)	0.85	0.95	0.78
Al(7)	0.84	0.74	0.91
Al(8)	0.75	0.78	0.85
Al(9)	0.05	0.09	0.16
Al(10)	0.15	0.05	0.22
Al(11)	0.16	0.26	0.09
Al(12)	0.26	0.22	0.15
Al(13)	0.92	0.96	0.03
Al(14)	0.84	0.85	0.62
Al(15)	0.96	0.66	0.78
Al(16)	0.66	0.91	0.96
Al(17)	0.77	0.73	0.66
Al(18)	0.85	0.84	0.08
Al(19)	0.73	0.03	0.91
Al(20)	0.03	0.78	0.73
Al(21)	0.08	0.04	0.97
Al(22)	0.16	0.16	0.39
Al(23)	0.04	0.34	0.23
Al(24)	0.34	0.08	0.04
Al(25)	0.22	0.27	0.34
Al(26)	0.15	0.15	0.92
Al(27)	0.27	0.97	0.08
Al(28)	0.97	0.23	0.27
Al(29)	0.15	0.93	0.91
Al(30)	0.93	0.59	0.04
Al(31)	0.85	0.04	0.11
Al(32)	0.77	0.92	0.15
Al(33)	0.73	0.08	0.04
Al(34)	0.84	0.14	0.04
Al(35)	0.25	0.90	0.97
Al(36)	0.61	0.64	0.76
Al(37)	0.46	0.44	0.37
Al(38)	0.58	0.45	0.43
Al(39)	0.62	0.52	0.54

X-ray powder diffraction calculations on the model were performed with the program *LAZY-PULVERIX* (Yvon, Jeitschko & Parthé, 1977) (Figs. 9*a*, *b*). The calculation demonstrated the importance of including the 'glue' atoms for a realistic estimate of the diffraction intensities for the model. No attempts were made to

include manganese among the 'glue' atoms in the α'' structure in order to achieve the reported chemical composition for quasicrystals (Janot, Pannetier, Dubois, Houin & Weinland, 1988), nor was any refinement of atomic positions tried. Despite these limited efforts, the calculated X-ray powder diagram of the simple cubic model seems to fit with the published powder X-ray diagram as well as other published models. This may not be surprising since these are also based on MacKay icosahedra and seem to include similar intericosahedral vectors.

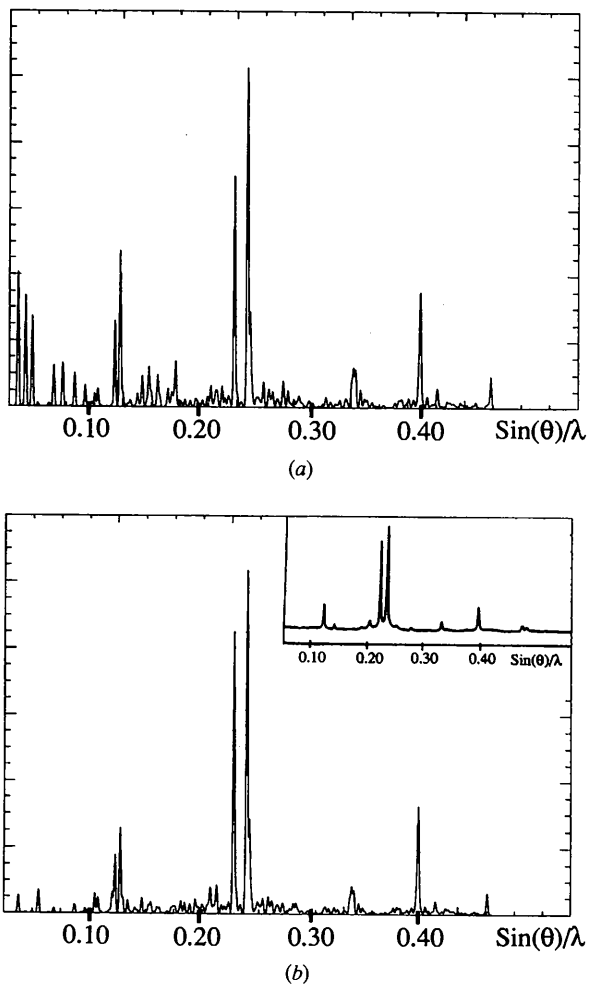

Fig. 9. Calculated powder intensities for α'' (*a*) without and (*b*) with 'glue' atoms included; published intensities for a quasicrystal are given in the insert (Yamamoto & Hiraga, 1988).

Thanks are due to A/S Hydro Aluminium, Årdal, for the alloy specimens. Projections of the structure model were photographed with the aid of the *SYBYL* (version 5.2) computer program from Tripos Associates. We are grateful to Chr. Rømming, Department of Chemistry, for help with use of this facility and to H. Fjellvåg for calculation of the powder X-ray data, also at Department of Chemistry, University of Oslo. Financial support from the Norwegian Research Council is gratefully acknowledged.

References

Adam, J. & Rich, J. B. (1954). *Acta Cryst.* **7**, 813–816.
Andersen, S. J., Guo, Y. X. & Høier, R. (1990). *Microbeam Analysis*, pp. 334–336. San Francisco Press.
Cahn, J. W., Gratias, D. & Mozer, B. (1988*a*). *Phys. Rev. B*, **38**, 1638-1642.
Cahn, J. W., Gratias, D. & Mozer, B. (1988*b*). *J. Phys. (Paris)*, **49**, 1225–1233.
Cheng, Y. F. & Gjønnes, J. (1994). *Acta Cryst.* A**50**, 455–461.
Cooper, M. & Robinson, K. (1966). *Acta Cryst.* **20**, 614–617.
Cowley, J. M. (1976). *Acta Cryst.* A**32**, 88–91.
Dmitrienko, V. E. (1993). *J. Non-Cryst. Solids*, **153&154**, 150–154.
Dmitrienko, V. E. (1994). *Acta Cryst.* A**50**, 515–526.
Duneau, M. & Oguey, C. (1989). *J. Phys. (Paris)*, **50**, 135–146.
Elser, V. & Henley, C. L. (1985). *Phys. Rev. Lett.* **55**, 2883–2886.
Gratias, D., Cahn, J. W. & Mozer, B. (1988). *Phys. Rev. B*, **38**, 1643–1646.
Guyot, P. & Audier, M. (1985). *Philos. Mag.* B**52**, L15–L19.
Hansen, V., Andersson, B., Tibballs, J. E. & Gjønnes, J. (1995). *Metall. Mater. Trans.* **26**B, 839–849.
Hansen, V., Gjønnes, J. & Andersson, B. (1989). *J. Mater. Sci. Lett.* **8**, 823–826.
Henley, C. L. & Elser, V. (1986). *Philos. Mag.* B**53**, L59–L66.
Hiraga, K. (1991). *J. Electron Microsc.* **40**, 81–91.
Janot, C., Pannetier, J., Dubois, J. M., Houin, J. P. & Weinland, P. (1988). *Philos. Mag.* **58**, 59–67.
Koskenmaki, D. C., Chen, H. S. & Rao, K. V. (1986). *Phys. Rev. B*, **33**, 5328–5332.
Mukhopadyay, N. K., Ishihara, K. N. & Ranganathan, S. (1991). *Acta Metall. Mater.* **39**, 1151–1159.
Nicol, A. D. I. (1953). *Acta Cryst.* **6**, 285–293.
Pannetier, J., Dubois, J. M., Janot, C. & Bilde, A. (1987). *Philos. Mag.* B**55**, 435–457.
Robertson, J. L & Moss, S. C. (1991). *Z. Phys.* B**83**, 391–405.
Shechtman, D., Blech, I., Gratias, D. & Cahn, J. W. (1984). *Phys. Rev. Lett.* **53**, 1951–1953.
Simensen, C. J., Fartum, P. & Andersen, A. (1984). *Fresenius Z. Anal. Chem.* **319**, 286–292.
Yamamoto, A. & Hiraga, K. (1988). *Phys. Rev. B*, **37**, 6207–6214.
Yvon, K., Jeitschko, W. & Parthé, E. (1977). *J. Appl. Cryst.* **10**, 73–74.